calculated by an ab initio SCF method using the GAUSSIAN 76 programs.

Acknowledgment. The authors thank D. Borchardt for assistance with the electrochemistry, Professor K. Hipps for assistance in obtaining the Raman data, and Professor R. Poshusta and Dr. R. Knochenmuss for assistance with the GAUSSIAN 76 programs. This work was supported by National Science Foundation Grant CHE-8204-102.

Registry No. $Mn(CNCH_3)_6BF_4$, 91281-18-4; $Mn(CNCH_3)_6(BF_4)_2$, 95979-49-0; $Mn(CNC_2H_5)_6BF_4$, 91281-19-5; $Mn(CNC_2H_5)_6(BF_4)_2$, 95979-50-3; $Mn(CNC_3H_7)_6BF_4$, 95979-42-3; $Mn(CNC_3H_7)_6(BF_4)_2$, 95979-52-5; $Mn(CNC_4H_9)_6BF_4$, 95979-44-5; $Mn(CNC_4H_9)_6(BF_4)_2$, 95979-54-7; $Mn(CNC_6H_{11})_6BF_4$, 89463-46-7; $Mn(CNC_6H_{11})_6(BF_4)_2$, 89463-47-8; $Mn(CNCH_2C_6H_5)_6BF_4$, 95979-45-6; $Mn(CNCH_2C_6H_5)_6(BF_4)_2$, 95979-55-8; $Mn(CNC_6H_5)_6BF_4$, 95979-46-7; $Mn(CNC_6H_5)_6(BF_4)_2$, 95979-56-9; $Mn(CNC_6H_4CH_3)_6BF_4$, 95979-47-8; $Mn(CNC_6H_4CH_3)_6(BF_4)_2$, 95979-57-0; $Mn(CNC_6H_4OCH_3)_6BF_4$, 95979-48-9; $Mn(CNC_6H_4OCH_3)_6(BF_4)_2$, 95979-58-1.

Supplementary Material Available: Tables of atomic coordinates and π_x^* and π_y^* orbital wave functions and unpolarized Raman spectra (24 pages). Ordering information is given on any current masthead page.

Contribution from the Department of Chemistry,
University of Missouri—Columbia, Columbia, Missouri 65211

Reactions of WCl_2L_4 (L = a Phosphine). 2.[1] Tungsten(IV) and Tungsten(V) Hydride Complexes

PAUL R. SHARP* and KEVIN G. FRANK

Received August 22, 1984

Oxidative addition of H_2 to $WCl_2(PMe_3)_4$ gives quantitative yields of $WCl_2H_2(PMe_3)_4$ (**1**). Chloride can be removed from **1** by $AlCl_3$ or $TlBF_4$ to give $[WClH_2(PMe_3)_4]^+$ (**2**). In MeCN, the reaction of **1** with $TlBF_4$ gives $[WCl(MeCN)H_2(PMe_3)_4]^+$ (**3**). By NMR spectroscopy and cyclic voltammetry, **1** and **3** are found to be in equilibrium in MeCN ($K = 0.1$). Both **1** and **3** can be oxidized to $\mathbf{1}^+$ and $\mathbf{3}^+$, which are also in equilibrium ($K = 4 \times 10^{-6}$). Chemical oxidation of **1** can be accomplished with Ag^+ or $FeCp_2^+$, but only $\mathbf{1}^+$ is isolated. The oxidation of the BF_4^- salt of **3** in the absence of Cl^- gives $\mathbf{3}^+$. A crystal structure determination of a sample of $\mathbf{1}^+$, prepared with $FeCp_2BF_4$, was performed. The crystals are orthorombic (*Pbca*) with $a = 12.371$ (2) Å, $b = 19.328$ (8) Å, $c = 27.339$ (4) Å, $V = 6536.9$ (1) Å^3, and $Z = 8$. The three-dimensional X-ray data were measured with the θ–2θ scan technique with a scintillation detector. The structure was resolved by Patterson and Fourier methods and refined by full-matrix least-squares calculations to give $R(F_o) = 0.055$ and $R_w(F_o) = 0.062$ for 1733 observations above 2σ. The solid-state structure consists of monomeric cations and anions with ferrocene of crystallization. The hydride ligands were not located.

Introduction

The polyhydrides of molybdenum(IV) and tungsten(IV) have received attention for many years for reasons ranging from their fluxional behavior to their potential as reducing agents.[2-4] Simple high-yield preparations for these complexes are scarce. In addition, the majority of the members of this group are of the type MH_4L_4 (L = a phosphine). Cationic ($MH_xL_yL'z$; L' = MeCN) and neutral ($MX_2H_2L_n$; X = CF_3CO_2 or *p*-$MeC_6H_4SO_3$) derivatives have been prepared by reactions of the present hydrides, MH_4L_4, with various acids and solvents.[3,5-7] Another member, $WCl_2H_2(PMe_2Ph)_4$, has been prepared in low yield by reducing $WCl_4(PMe_2Ph)_3$ in THF with Mg.[8]

Recent attention has focused on improved preparations and attempts to prepare new members. Recently, an unsuccessful attempt to increase reactivity by oxidation of MoH_4L_4 to a paramagnetic molybdenum(V) hydride complex was reported.[3] (Few paramagnetic hydrides are known so their reactivity has not been fully explored.) In this paper we report the simple, high-yield preparation of $WCl_2H_2(PMe_3)_4$ (**1**), by simple oxidative addition of H_2 to $WCl_2(PMe_3)_4$. In addition, several derivatives of **1** can be readily obtained by halide abstraction. However, most interesting is the electrochemical behavior of **1** in MeCN: Two reversible one-electron-oxidation waves were observed, corresponding to the oxidation of **1** and its MeCN solvate, $[WCl(MeCN)H_2(PMe_3)_4]^+$ (**3**), to paramagnetic hydride complexes.

Scheme I

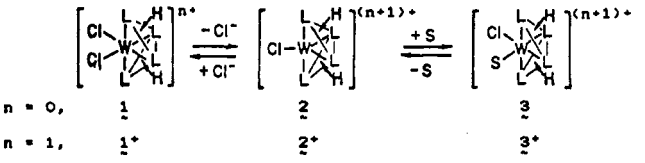

Results

Preparation and Characterization of $WCl_2H_2(PMe_3)_4$ (1). Orange $WCl_2(PMe_3)_4$ reacts readily with H_2 at 60 °C to give yellow $WCl_2H_2(PMe_3)_4$ (**1**; eq 1) quantitatively (96% isolated

$$WCl_2(PMe_3)_4 + H_2 \rightarrow \underset{\mathbf{1}}{WCl_2H_2(PMe_3)_4} \qquad (1)$$

yield). Unlike the related tetrahydrides, this diamagnetic complex is apparently static on the NMR time scale; two sets of phosphines and one set of hydrides are observed by ^{31}P and ^1H NMR spectroscopy, respectively. The spectra do not change between −50 and +70 °C, and simulation of the hydride region of the ^1H NMR spectrum indicated a rigid $HH'AA'B_2$ spin system (see Experimental Section and Supplementary Figure S-1a,b). These data are consistent with a dodecahedral geometry, the same geometry found for all other members of this group as well as the recently reported tantalum analogue of **1**.[9] An alternative and convenient, though not exact, description of this geometry is that of a distorted bi-face-capped octahedron. This representation of the structure of **1** is shown in Scheme I.

To further establish the presence of the hydride ligands, **1** was treated with $CDCl_3$. While a reaction did occur, little or no

(1) Part 1: Sharp, P. R. *Organometallics* **1984**, *3*, 1217-1223.
(2) Meakin, P.; Guggenberger, L. T.; Peet, W. G.; Muetterties, E. L.; Jesson, J. P. *J. Am. Chem. Soc.* **1973**, *95*, 1467-1474.
(3) Rhodes, L. F.; Zubkowski, J. D.; Folting, K.; Huffman, J. C.; Caulton, K. C. *Inorg. Chem.* **1982**, *21*, 4185-4192.
(4) Crabtree, R. H.; Hlatky, G. G. *Inorg. Chem.* **1982**, *21*, 1273-1275.
(5) Crabtree, R. H.; Hlatky, G. G.; Parnell, C. P.; Segmuller, B. E.; Uriarte, R. J. *Inorg. Chem.* **1984**, *23*, 354-358.
(6) Chiu, K. W.; Jones, R. A.; Wilkinson, G.; Galas, A. M. R.; Hursthouse, M. B.; Malik, K. M. A. *J. Chem. Soc., Dalton Trans.* **1981**, 1204-1211.
(7) Carmona-Guzzman, E.; Wilkinson, G. *J. Chem. Soc., Dalton Trans.* **1977**, 1716-1721.
(8) Fakley, M. E.; Richards, R. L. *Transition Met. Chem. (Weinheim, Ger.)* **1982**, *7*, 1.
(9) Luetkens, M. L., Jr.; Huffman, J. C.; Sattelberger, A. P. *J. Am. Chem. Soc.* **1983**, *105*, 4474-4475. Luetkens, M. L., Jr.; Elcesser, W. L.; Huffman, J. C.; Sattelberger, A. P. *Inorg. Chem.* **1984**, *23*, 1718-1726.

0020-1669/85/1324-1808$01.50/0

$CDHCl_2$ was observed by ^1H NMR spectroscopy. Instead, a complex series of changes occurred, ending ultimately (16 h) in the production of several paramagnetic species. The reaction of **1** with CCl_4 in C_6D_6 gave similar results; no $CHCl_3$ was observed. Curiously, we have been unable to find any reports of the reactions of other hydrides in this group with chlorinated solvents, a reaction often used to characterize hydride complexes.[10]

A common reaction of polyhydride complexes, including the tungsten and molybdenum tetrahydride complexes, is thermal or photolytic reductive elimination of H_2.[11] For **1**, no change was observed in its ^1H NMR spectrum after heating (80 °C) or irradiation (9 W, low-pressure Hg lamp, quartz tube) in C_6D_6 for 24 h. Under more forceful photolytic conditions (450 W, medium-pressure Hg lamp) **1** is slowly converted (24 h) to a mixture of products, one of which is $WCl_2(PMe_3)_4$ (ca. 50%), the expected elimination product. The UV–vis spectrum of **1** is very similar to that reported for $MH_4(dppe)_2$ (dppe = 1,2-bis(diphenylphosphino)ethane), which readily eliminates H_2 under photolysis.[11b] The related rhenium hydride complexes $ReH_3(PPh_2Me)_4$[13] and $ReH_5(PPh_2Me)_3$[12,13] do not eliminate H_2.

In refluxing Bu_2O, **1** slowly decomposed (16 h) to an unidentified brown solid. While no attempt was made to check for evolved H_2, simple elimination must not have occurred since the expected elimination product $WCl_2(PMe_3)_4$ is known to give green $W_2Cl_4(PMe_3)_4$ under these conditions.[14] In the solid state **1** melts with decomposition at 145 °C. Unfortunately, the effect of the chlorides in **1** cannot be assessed since no data on known $WH_4(PMe_3)_4$ are available.[6]

Halide Abstraction Reactions. $WCl_2H_2(PMe_3)_4$ reacts with $TlBF_4$ in chlorobenzene or THF to give blue, 16-electron, $[WClH_2(PMe_3)_4]^+BF_4^-$ (**2a**; eq 2), which can be separated from

$$WCl_2H_2(PMe_3)_4 + TlBF_4 \rightarrow \underset{\textbf{2a}}{[WClH_2(PMe_3)_4]^+BF_4^-} + TlCl \quad (2)$$

TlCl by extraction into 1,2-dichloroethane at −30 °C. (At higher temperatures **2a** reacts with the solvent.) A similar reaction occurs between **1** and $AlCl_3$ in ether to give a blue product (**2b**) with NMR spectra (^1H and ^{31}P) identical with those of **2a** and a very similar IR spectrum. This product must be the $AlCl_4^-$ salt of $[WClH_2(PMe_3)_4]^+$ (**2**). On the basis of NMR spectroscopy, **2** contains two different phosphine ligands and two equivalent hydride ligands. Simulation of the hydride region of the ^1H NMR spectrum indicated an $HH'AA'B_2$ spin system (see the Experimental Section and Supplementary Figure S-1c,d). As a 7-coordinate system, **2** might be expected to display fluxional behavior. Unfortunately, the temperature dependence of the NMR spectra could not be investigated because of the reaction of **2** with the solvent. A reasonable structure for **2** is shown in Scheme I. This structure was observed (X-ray) for the neutral, isoelectronic tantalum analogue of **2**, which is apparently formed by the spontaneous loss of chloride from the isoelectronic, anionic, tantalum analogue of **1**.[9] Again, a convenient, though not exact, description of this structure is that of a bi-face-capped trigonal bipyramid (see Scheme I). This can be considered a derivative of the bi-face-capped octahedron of **1** obtained by the removal of a chloride ligand.

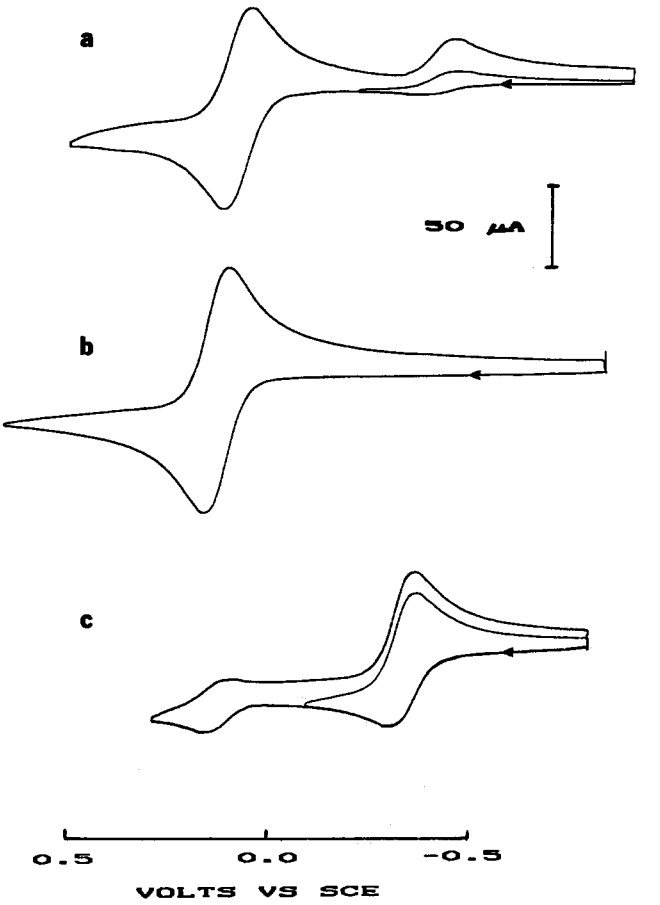

Figure 1. Cyclic voltammograms at a Pt disk electrode (0.02 cm^2) in MeCN (23 °C; scan rate 500 mV s^{-1}; 0.2 M $(TBA)PF_6$): (a) $WCl_2H_2(PMe_3)_4$ (**1**), 8.9 mM; (b) $[WCl(MeCN)H_2(PMe_3)_4]^+BF_4^-$ (**3a**), 8.4 mM; (c) same conditions as for curve b but with 20 equiv of NEt_4Cl added.

Scheme II

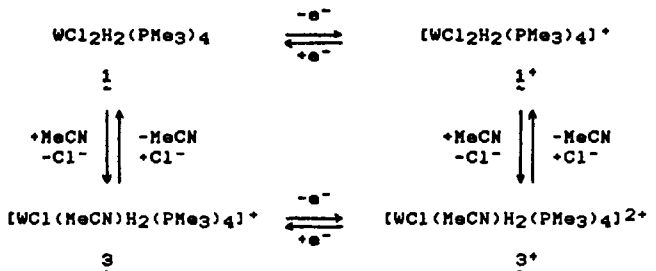

If **1** is treated with $TlBF_4$ in MeCN, instead of THF or chlorobenzene, yellow $[WCl(MeCN)H_2(PMe_3)_4]^+BF_4^-$ (**3a**; eq 3) is

$$WCl_2H_2(PMe_3)_4 + TlBF_4 \xrightarrow{MeCN} \underset{\textbf{3a}}{[WCl(MeCN)H_2(PMe_3)_4]^+BF_4^-} \quad (3)$$

obtained. (Isolated **2a** gives the same product when dissolved in MeCN.) This species is fluxional on the NMR time scale. Slow-exchange NMR spectra (^1H and ^{31}P), obtained at −20 °C, show three different phosphine ligands in a ratio of 1:1:2. The two most similar phosphorus signals collapse and coalesce as the temperature is raised, probably due to dissociation of MeCN and re-formation of **2** (see Scheme I). This process apparently does occur since facile exchange of CD_3CN for coordinated CH_3CN is observed by NMR spectroscopy. The CN stretch was not detected by IR spectroscopy, but the WH stretch was observed at 1960 cm^{-1}. A structure for **3**, consistent with these data, is shown in Scheme I.

Cyclic Voltammetry. A typical cyclic voltammogram (CV) at a Pt disk electrode of an 8.9 mM solution of **1** in MeCN is shown

(10) For examples of reactions of hydride complexes with organic halides see: (a) Calado, J. C. G.; Dias, A. R.; Martinho Simoes, J. A. *J. Organomet. Chem.* **1979**, *174*, 77–80. (b) Davies, S.; Green, M. L. H. *J. Chem. Soc., Dalton Trans.* **1978**, 1510. (c) Jones, R. A.; Chiu, K. W.; Wilkinson, G. *J. Chem. Soc., Chem. Commun.* **1980**, *408*. (d) Alper, H. *Tetrahedron Lett.* **1975**, *27*, 2257. (e) Green, M. L. H.; Jones, D. J. *Adv. Inorg. Chem. Radiochem.* **1965**, *7*, 115.

(11) (a) Geoffroy, G. L.; Wrighton, M. S. "Organometallic Photochemistry"; Academic Press: New York, 1979. (b) Graff, J. L.; Sobieralski, T. J.; Wrighton, M. S.; Geoffroy, G. L. *J. Am. Chem. Soc.* **1982**, *104*, 7526–7533. (c) Archer, L. J.; George, T. A. *Inorg. Chem.* **1979**, *18*, 2079–2082.

(12) Roberts, D. A.; Geoffroy, G. L. *J. Organomet. Chem.* **1981**, *214*, 221.

(13) Green, M. A.; Huffman, J. C.; Caulton, K. G. *J. Am. Chem. Soc.* **1981**, *103*, 695.

(14) Sharp, P. R.; Schrock, R. R. *J. Am. Chem. Soc.* **1980**, *102*, 1430.

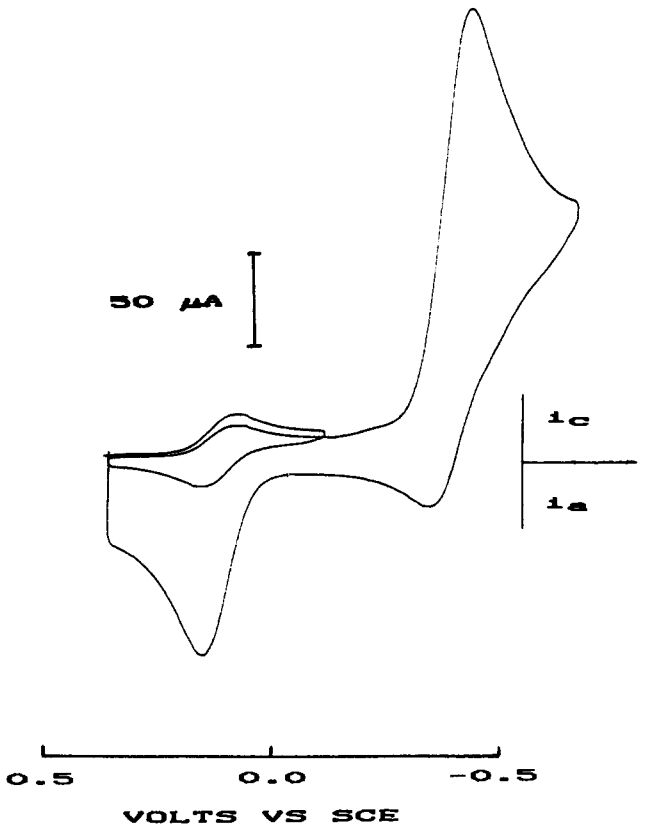

Figure 2. Cyclic voltammogram at a Pt disk electrode (0.03 cm^2) in MeCN (23 °C; scan rate 500 mV s^{-1}; 0.i M (TBA)PF_6) of a 15 mM solution of **1** after complete coulometric oxidation at 0.3 V vs. SCE.

in Figure 1a. The CV can be explained by introducing the equilibrium reactions shown in Scheme II. The two oxidation waves thus correspond to the oxidation of **1** and **3**, which are in equilibrium in MeCN, most likely through the intermediacy of **2** (Scheme I). The two oxidation waves can be assigned by examining the CV of **3a** (the BF_4^- salt of **3**) in the absence of Cl^- (Figure 1b). In this case only the oxidation of **3** at 0.14 V vs. SCE is observed, and it corresponds to a reversible one-electron Nernstian process ($E_{1/2}$ = 0.11 V vs. SCE). Alternatively, the system can be loaded with Cl^- (Figure 1c), which shifts the equilibrium between **1** and **3** toward **1**. The oxidation of **1** to $\mathbf{1}^+$ at −0.37 V vs. SCE then corresponds essentially to a reversible one-electron Nernstian process ($E_{1/2}$ = −0.40 V vs. SCE). In Figure 1a this leads to the assignment of the small wave at −0.37 V vs. SCE to the oxidation of **1** and the larger wave at 0.14 V vs. SCE to the oxidation of **3**. This assignment seems reasonable on the basis of charge arguments; neutral **1** should be easier to oxidize than cationic **3**. If we assume that **1** and **3** have similar diffusion coefficients and that the coupled chemical reactions do not significantly affect the peak currents, the equilibrium constant, K, for $\mathbf{1} \rightleftarrows \mathbf{3}$ is 0.09. The ^1H and ^{31}P NMR spectra of **1** in MeCN also show an equilibrium mixture of **1** and **3**. By integration of the ^{31}P NMR spectrum and with equal relaxation times assumed for the ^{31}P nuclei of **1** and **3**, K = 0.1 for $\mathbf{1} \rightleftarrows \mathbf{3}$, in good agreement with the CV result.

An additional feature of the CV of **1** to note is the increased size of the return reduction wave for **1** ($\mathbf{1}^+ \rightarrow \mathbf{1}$) when the sweep is reversed after the oxidation of **3** (Figure 1a). This suggests that following the oxidation of **3** to $\mathbf{3}^+$ some $\mathbf{3}^+$ converts to $\mathbf{1}^+$, contributing to the concentration of $\mathbf{1}^+$ available for reduction at the electrode surface. This would be expected to occur if the equilibrium between $\mathbf{1}^+$ and $\mathbf{3}^+$ favors $\mathbf{1}^+$ more the **1** was favored in the equilibrium between **1** and **3**. This is found to be the case (see below and Figure 2).

Controlled-Potential Coulometry. Controlled-potential coulometry (CPC) at 0.3 V vs. SCE on a 15 mM solution of **1** in MeCN proceeded smoothly to give a red solution and an n(app) (faradays per mole of reactant) of 1.02. A CV of this red solution at a Pt disk electrode is shown in Figure 2. The major species is now the MeCN-free complex $\mathbf{1}^+$. With the same assumptions as above, $K = 4 \times 10^{-6}$ for $\mathbf{1}^+ \rightleftarrows \mathbf{3}^+$. The difference between the equilibrium constants for $\mathbf{1} \rightleftarrows \mathbf{3}$ and $\mathbf{1}^+ \rightleftarrows \mathbf{3}^+$ might be expected since the loss of Cl^- from neutral **1** should be much easier than the loss of Cl^- from cationic $\mathbf{1}^+$. Only $\mathbf{1}^+$ was isolated from the chemical oxidation of **1** in MeCN (see below). A CV of a chemically prepared sample of $\mathbf{1}^+$ showed identical behavior.

Chemical Preparation of $[WCl_2H_2(PMe_3)_4]^+$ ($\mathbf{1}^+$). Chemical oxidation of an MeCN solution of **1** with ferrocenium ion gives a red solution from which red crystals can be isolated. Elemental analysis, NMR spectroscopy, and an X-ray crystal structure determination showed these to be $[WCl_2H_2(PMe_3)_4]^+BF_4^-\cdot Cp_2Fe$ i.e. crystals of $\mathbf{1}^+$ with a ferrocene of crystallization (eq 4).

$$WCl_2H_2(PMe_3)_4 + Cp_2Fe^+BF_4^- \rightarrow [WCl_2H_2(PMe_3)_4]^+BF_4^-\cdot Cp_2Fe \quad (4)$$

Ferrocene-free material can be obtained if the reaction is conducted in toluene (see Experimental Section). (Ag^+ also seemed to work, but the reaction was not as clean probably due to competing precipitation of AgCl to form **3**.)

To confirm the chemical reversibility of the oxidation of **1**, an MeCN solution of ferrocene-free $\mathbf{1}^+$ was treated with Na/Hg. However, **3** and not **1** was obtained (eq 5). This result can be

$$[WCl_2H_2(PMe_3)_4]^+BF_4^- + Na/Hg \rightarrow [WCl(MeCN)H_2(PMe_3)_4]^+BF_4^- + NaCl \quad (5)$$

explained by considering the equilibrium between $\mathbf{1}^+$ and $\mathbf{3}^+$, the greater ease of reduction of $\mathbf{3}^+$ over $\mathbf{1}^+$, and the lower solubility in MeCN of NaCl over $NaBF_4$.

Chemical Preparation of $[WCl(MeCN)H_2(PMe_3)_4]^{2+}$ ($\mathbf{3}^+$). Chemical oxidation of **3a** with $AgBF_4$ in MeCN cleanly gives a red solution from which orange crystals of $[WCl(MeCN)H_2(PMe_3)_4]^{2+}(BF_4^-)_2$ ($\mathbf{3a}^+$) can be isolated (eq 6). Like its parent

$$[WCl(MeCN)H_2(PMe_3)_4]^+BF_4^- + AgBF_4 \rightarrow [WCl(MeCN)H_2(PMe_3)_4]^{2+}(BF_4^-)_2 + Ag \quad (6)$$

3, $\mathbf{3}^+$ exchanges CH_3CN with CD_3CN: Free CH_3CN is the only signal observed in its ^1H NMR spectrum in CD_3CN. The exchange, and also the equilibrium between $\mathbf{1}^+$ and $\mathbf{3}^+$, most likely occurs through the intermediacy of $\mathbf{2}^+$ (Scheme I), a 15-electron, unsaturated, paramagnetic hydride complex.

EPR Spectra. The X-band EPR spectrum for $\mathbf{1}^+$ in MeCN is shown in Figure 3a. At first examination, on the basis of the CV results, we might assign the more intense low-field signal (g = 2.00) to $\mathbf{3}^+$ and the higher field signal (g = 1.95) to $\mathbf{1}^+$. The spectrum of pure $\mathbf{3}^+$ is shown in Figure 3b, and though the appearance of the signal is slightly different from that of the low-field signal in Figure 3a, this does tend to confirm the assignment. Indeed, the addition of 1 equiv of chloride (NEt_4Cl) to $\mathbf{3}^+$ regenerates the spectrum in Figure 3a. However, the addition of excess chloride, which increases the concentration of $\mathbf{1}^+$, does not cause the high-field signal to grow. Instead, it disappears altogether and the lower field signal remains relatively constant.

Ignoring for the moment the high-field signal, we may summarize our observations as follows. In the two limits of pure $\mathbf{3}^+$ (no free chloride) and nearly pure $\mathbf{1}^+$ (excess free chloride) a single signal is observed for each, and each has nearly the same g value and nearly the same hyperfine splittings. (This is perhaps not too surprising since for the chloride and MeCN to be lost so readily the MO involved must be predominantly ligand centered.) A mixture of $\mathbf{1}^+$ and $\mathbf{3}^+$, as we must have in Figure 3a, would therefore not be readily distinguishable from pure $\mathbf{1}^+$ or pure $\mathbf{3}^+$. Using a simulation program,[15] we have been able to reproduce the spectrum observed for $\mathbf{1}^+$. As expected from the solid-state structure, coupling to two sets of two phosphines ($\langle a \rangle$ = 25 and 22 G) and two hydrides ($\langle a \rangle$ = 10 G) was required (line width = 10 G). This is in contrast to the spectrum of the tantalum

(15) Ahn, M. K. *QCPE* **1966**, *11*, 83.

Table I. Crystallographic and Data Collection Parameters[a]

space group	*Pbca*	diffractometer	Enraf-Nonius CAD-4
a, Å	12.371 (2)	cryst size, mm	0.1 × 0.2 × 0.3
b, Å	19.327 (8)	λ, Å (Mo Kα)	0.71073
c, Å	27.339 (4)	μ, cm^{-1}	44.2; transmission range 89.3–99%
V, $Å^3$	6536.9 (1)	scan speed	variable to maintain 3% counting stats to a max time of 120 s/scan
π_{calcd}	1.35	θ–2θ scan	96 steps/scan
Z	8	bkgd	16 steps on each side of peak
$R(F_o)$	0.055	peak	64 steps
$R_w(F_o)$	0.062	takeoff angle, deg	2.8
no. of reflcns measured	3541	scan width in θ, deg	0.70 + 0.35 tan θ
no. of unique data	3035	2θ max, deg	40.0
no. of data above 2σ	1733	*khl* range	$+h,+k,+l$
no. of params refined	271	decay cor range	0.98–1.23

[a] Here and in the following tables the numbers in parentheses represent the error in the least significant digit(s).

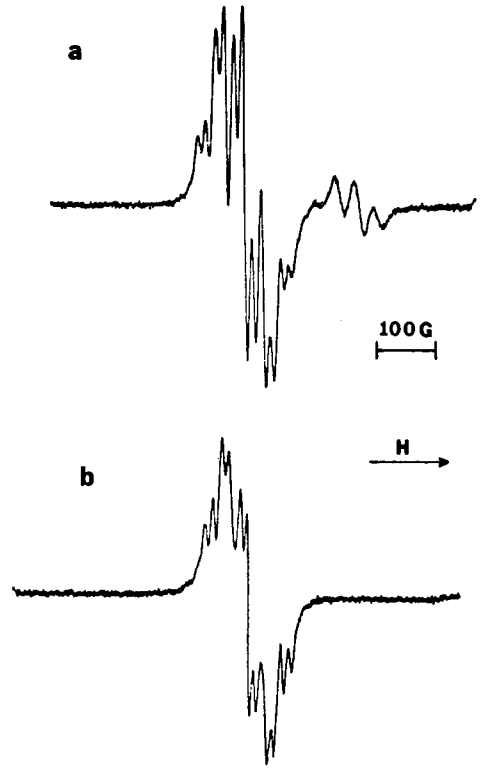

Figure 3. EPR spectra in MeCN: (a) $[WCl_2H_2(PMe_3)_4]^+BF_4^-$ (1^+); (b) $[WCl(MeCN)H_2(PMe_3)_4]^+BF_4^-$ ($\mathbf{3a}^+$).

analogue, where either the difference between the coupling of the two sets of phosphines was too small to resolve or the molecule was fluxional on the EPR time scale.[9,16]

The question now remains as to the nature of the high-field signal in Figure 3a. Since it is only present when there is a mixture of $\mathbf{1}^+$ and $\mathbf{3}^+$, we propose that the species responsible for this signal is a chloride-bridged dimer of $\mathbf{1}^+$ and $\mathbf{3}^+$ (eq 7). This species

$$[WCl_2H_2(PMe_3)_4]^+ + [WCl(MeCN)H_2(PMe_3)_4]^{2+} \rightleftarrows [(WClH_2(PMe_3)_4)_2Cl]^{3+} + MeCN \quad (7)$$

would not be detectable by CV if it is in rapid equilibrium with $\mathbf{1}^+$ and $\mathbf{3}^+$.

Solid-State Structure of $[WCl_2H_2(PMe_3)_4]^+BF_4^-\cdot Cp_2Fe$. The experimental parameters and the crystal data are given in Table I. Table II gives the refined atom fractional coordinates and Table III gives selected bond distances and angles.

The structure consists of discrete cations, disordered BF_4 anions, and ferrocenes of crystallization. The cationic portion of the structure is shown in Figure 4, and a packing diagram, including the ferrocenes of crystallization, is available as Supplementary Figure S-2. Although the hydride ligands were not found, the two orthogonal trapezoidal ligand planes of the dodecahedral geometry are still easily located. The first plane is defined by P1, P2, Cl1, and Cl2 (maximum deviation from least-squares plane = –0.227 Å), and the second is defined by P3, P4, and the missing

(16) We thank Professor A. P. Sattelberger for giving us these results prior to publication.

Table II. Positional Parameters for Refined Atoms

atom	*x*	*y*	*z*	*B*, $Å^2$
W	0.28672 (7)	0.64446 (5)	0.12887 (3)	3.17 (2)
Fe	0.7423 (3)	0.3994 (2)	0.1667 (1)	3.89 (8)
Cl1	0.3495 (6)	0.5331 (4)	0.1594 (3)	7.2 (2)
Cl2	0.3850 (5)	0.6915 (4)	0.1987 (2)	5.7 (2)
P1	0.2230 (5)	0.7665 (3)	0.1287 (2)	4.2 (1)
P2	0.2313 (5)	0.5714 (4)	0.0585 (3)	4.8 (2)
P3	0.4766 (5)	0.6528 (4)	0.0897 (2)	3.8 (2)
P4	0.1308 (5)	0.6166 (4)	0.1892 (2)	4.4 (2)
C1R1	0.812 (2)	0.491 (1)	0.1810 (9)	5.0 (7)
C1P1	0.163 (2)	0.807 (2)	0.187 (1)	7.9 (9)
C1R2	0.621 (2)	0.362 (1)	0.2072 (9)	6.3 (7)
C1P2	0.103 (2)	0.520 (1)	0.072 (1)	7.8 (9)
C1P3	0.567 (2)	0.582 (2)	0.104 (1)	6.3 (8)
C1P4	–0.004 (2)	0.650 (1)	0.1740 (8)	4.4 (6)
C2R1	0.840 (2)	0.472 (1)	0.1324 (9)	5.7 (7)
C2P1	0.127 (2)	0.791 (2)	0.814 (9)	7.1 (8)
C2R2	0.665 (2)	0.307 (1)	0.179 (1)	7.7 (9)
C2P2	0.191 (2)	0.615 (2)	0.0045 (9)	7.7 (9)
C2P3	0.481 (2)	0.658 (2)	0.0252 (9)	8 (1)
C2P4	0.161 (2)	0.650 (2)	0.2535 (8)	10 (1)
C3P1	0.334 (2)	0.831 (1)	0.118 (1)	7.7 (9)
C3R1	0.891 (2)	0.408 (1)	0.137 (1)	5.5 (7)
C3R2	0.659 (2)	0.326 (1)	0.130 (1)	6.2 (7)
C3P2	0.322 (2)	0.506 (1)	0.038 (1)	7.3 (8)
C3P3	0.557 (2)	0.723 (1)	0.105 (1)	9 (1)
C3P4	0.098 (3)	0.527 (1)	0.203 (1)	8.8 (9)
C4R1	0.902 (2)	0.389 (1)	0.187 (1)	5.4 (7)
C4R2	0.607 (2)	0.391 (1)	0.1275 (9)	4.5 (6)
C5R1	0.851 (2)	0.443 (1)	0.2149 (9)	5.7 (7)
C5R2	0.582 (2)	0.409 (1)	0.177 (1)	5.0 (7)

Table III. Selected Interatomic Distances and Angles

bond distances (Å)			bond angles (deg)			
atom 1	atom 2	dist	atom 1	atom 2	atom 3	angle
W	Cl1	2.436 (6)	Cl1	W	Cl2	84.4 (2)
W	Cl2	2.439 (6)	Cl1	W	P1	160.0 (2)
W	P1	2.487 (5)	Cl1	W	P2	81.4 (2)
W	P2	2.482 (6)	Cl1	W	P3	84.7 (2)
W	P3	2.586 (5)	Cl1	W	P4	80.5 (2)
W	P4	2.595 (5)	Cl2	W	P1	78.8 (2)
P1	C1P1	1.93 (3)	Cl2	W	P2	162.9 (2)
P1	C2P1	1.82 (2)	Cl2	W	P3	81.2 (2)
P1	C3P1	1.88 (2)	Cl2	W	P4	87.2 (2)
P2	C1P2	1.91 (2)	P1	W	P2	116.8 (2)
P2	C2P2	1.78 (2)	P1	W	P3	103.2 (2)
P2	C3P2	1.79 (2)	P1	W	P4	87.8 (2)
P3	C1P3	1.81 (2)	P2	W	P3	88.0 (2)
P3	C2P3	1.77 (2)	P2	W	P4	99.7 (2)
P3	C3P3	1.73 (2)	P3	W	P4	162.0 (2)
P4	C1P4	1.83 (2)				
P4	C2P4	1.91 (2)				
P4	C3P4	1.82 (2)				

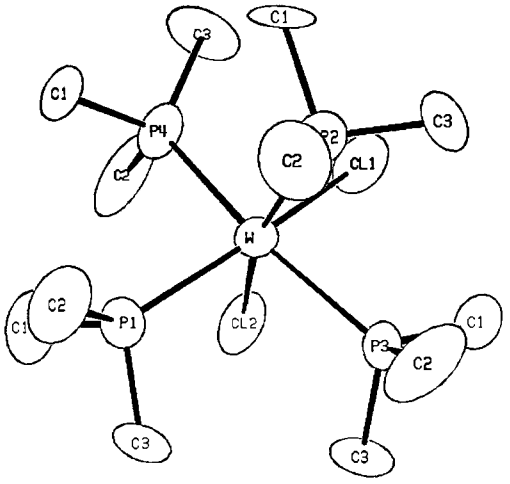

Figure 4. ORTEP drawing of 1^+ in $[WCl_2H_2(PMe_3)_4]^+BF_4^-\cdot Cp_2Fe$ (50% probability ellipsoids).

hydride ligands. Since the tungsten atom is at the center of these planes (distance to first plane = 0.018 Å), its position can be used to define the plane with the missing hydrides. The angle between these planes is 86.1°, close to the required 90°. An essentially identical angle (85.9°) was found in the isoelectronic tantalum complex.[9]

For the purpose of visualizing the position of the hydride ligands, the alternative description of the structure as a distorted bi-face-capped octahedron is perhaps best. The hydride ligands could then be described as occupying the two faces formed by P4, P2, P1 and P3, P2, P1 (see Scheme I).

The major differences between the present structure and that of the tantalum analogue can be attributed to the smaller radius of tungsten(V) as opposed to the radius of tantalum(IV). With the shorter M–Cl distances (2.44 vs. 2.55 Å), the Cl–M–Cl angle must increase (84.4 vs. 81.8°) to maintain the Cl–Cl distance (3.23 Å for 1^+) near the sum of the van der Waals radii (ca. 3.40 Å). This forces P2 and P3 closer together (116.8 vs. 123.6°). The P3–M–P4 angle increases slightly (162.0 vs. 158.0°) as P3 and P4 bend further back from P1 and P2.

The remaining features of the structure are ordinary, with perhaps the exception of the ferrocene of crystallization. (Proton NMR data show that it is neutral ferrocene and not ferrocenium.) While solvents of crystallization are common, it is usual to encounter an organometallic of crystallization.

Discussion

The most notable feature of the present work is the facile oxidation of **1** and **3** to *stable*, paramagnetic, cationic hydride complexes. Previous work has shown that while many paramagnetic hydrides can be generated, few are stable enough to observe or isolate.[17-21] Decomposition was shown to occur by ejection of a proton in two cases and by net reductive elimination of H_2 in others although this may also occur by preliminary ejection of H^+.[17]

A factor involved in the stability of 1^+ and 3^+ may be the presence of the chloride ligands. The stabilizing effect of halide (and alkyl) substitution for hydride on the stability of paramagnetic metal complexes has been noted.[17] While the greater stability of the alkyl- and chloride-substituted hydride complexes may be attributed to blocking reductive elimination of H_2, increased stability was observed even in cases where decomposition occurred by proton ejection. The change in electron density on the metal was evidently not involved since no correlation between stability and oxidation potential was observed.

All of the factors involved in the stabilization of paramagnetic hydride complexes remain to be found and interpreted. However, the stability of paramagnetic hydride complexes is evidently reflected in the reactivity of the hydride ligands since the few known stable paramagnetic hydride complexes and/or their diamagnetic parents are noted for their inert hydride ligands.[18,19] This is exemplified by the thermolysis of $TaCl_2H_2(PMe_3)_4$, which appears to proceed by breakage of a Ta–P bond and *not* a Ta–H bond.[9] In the present study, the lack of H/Cl exchange when **1** is treated with $CDCl_3$ or CCl_4 and the resistance of **1** to reductive elimination similarly suggest inert hydride ligands.

Experimental Section

General Procedures. Atmospheric-pressure experiments were performed under a dinitrogen atmosphere in a VAC drybox or by Schlenk technique. Pressure experiments were performed in a Lab-Crest pressure bottle. Solvents were dried and purified by standard techniques under dinitrogen. $WCl_2(PMe_3)_4$ was prepared as previously reported.[1] $TlBF_4$ was prepared by adding solid $Tl_2(CO_3)$ to 50% HBF_4 with stirring. The resulting solid was washed with cold water and dried in vacuo. $FeCp_2BF_4$ was prepared from the reaction of ferrocene and $AgBF_4$ in CH_2Cl_2. Reagent grade, fresh, white, free-flowing $AlCl_3$ and $AgBF_4$ and CP grade hydrogen gas were used as received.

NMR shifts are reported in ppm referenced to Me_4Si for ^1H and ^{13}C NMR spectra and to external H_3PO_4 for ^{31}P NMR spectra. The ^{13}C NMR spectra were obtained in the gated decoupled mode except where noted. Only when the NMR spectra were run at relatively high fields or at temperatures different from 35 ± 5 °C are the particulars noted. The NMR simulation program was that supplied with the Nicolet 300 instruments. The UV–vis spectrum was recorded in a 1 cm path length quartz cell on a Cary 14 spectrometer. EPR spectra were recorded on a locally modified Varian 4500 spectrometer. Electrochemical studies were performed in conventional single- and three-compartment cells using platinum working and counter electrodes. An Ag quasi-reference electrode was used; however, all reported potentials are vs. SCE as determined by an internal ferrocene reference ($E_{1/2}$ = 0.31 V vs. SCE). The criteria for reversibility were based on the ΔE_p behavior of the ferrocene couple under our experimental conditions. The working CV and reference electrodes were polished with alumina (0.3 μm) on felt. The other electrodes were treated with concentrated nitric acid. Spectrograde MeCN was dried by vacuum distillation from P_2O_5. Tetra-*n*-butylammonium hexafluorophosphate ($(TBA)PF_6$) was prepared as previously described.[22] Microanalyses were performed by Schwarzkopf Microanalytical Laboratory using drybox techniques.

Preparation of $WCl_2H_2(PMe_3)_4$ (1). $WCl_2(PMe_3)_4$ (1.2 g, 2.11 mmol) in 5 mL of toluene was heated with stirring to 70 °C under 30 psi of H_2 pressure. After 16 h, the pressure was released and 5 mL of pentane was added. After 1 min, yellow crystals (0.45 g) were isolated by filtration. A second crop of 0.70 g was obtained by cooling the filtrate to −40 °C overnight; total yield = 1.15 g (96%). Very large octahedra were grown from saturated THF solutions cooled to −40 °C.

Anal. Calcd for $WC_{12}H_{40}Cl_2P_4$: C, 25.69; H, 6.83. Found: C, 25.90; H, 6.82. ^1H NMR (toluene-d_8, 270 MHz): 1.39 and 1.38 (overlapping t, 36 H, J = 3.4 Hz, 2 PMe_3 and 2 PMe_3'), −3.46 (m with satellites, ~2 H, J_{HW} = 12 Hz, WH_2; see Figure S-1a). Simulation of the hydride region as an $HH'AA'B_2$ spin system (Figure S-1b) gave J_{HA} = 43 Hz, $J_{HA'}$ = 36 Hz, J_{HB} = 63 Hz, and J_{AB} = 16 Hz. $^{31}P\{^1H\}$ NMR (toluene-d_8, 109 MHz): −21 (t with satellites, J_{PP} = 16 Hz, J_{PW} = 179 Hz, 2 PMe_3), −27 (t with satellites, J_{PP} = 16 Hz, J_{PW} = 201 Hz, 2 PMe_3'). When only the PMe_3 protons are decoupled, each signal splits into overlapping triplets. IR (Nujol; cm^{-1}): 1940 (s, br, WH). UV–vis (benzene, 23 °C): 375 nm (ϵ 1300 M^{-1} cm^{-1}).

Preparation of $[WClH_2(PMe_3)_4]^+X^-$ (2). (a) $X^- = BF_4^-$. Solid $TlBF_4$ (0.3 g, 1 mmol) was added to a vigorously stirred solution of $WCl_2H_2(PMe_3)_4$ (0.5 g, 0.89 mmol) in 5 mL of chlorobenzene. After 2 h, the blue product was removed by filtration, cooled to −40 °C, and extracted with cold (−40 °C) CH_2Cl_2, which was removed in vacuo while the solution was still cold; yield 0.48 g (88%).

Anal. Calcd for $WC_{12}H_{28}BClF_4P_4$: C, 23.53; H, 6.25. Found: C, 22.95; H, 5.95. The NMR data were identical with those of the $AlCl_4^-$ salt below. IR (Nujol; cm^{-1}): 1920 (m, br, WH).

(b) $X^- = AlCl_4^-$. $WCl_2H_2(PMe_3)_4$ (095 g, 0.89 mmol) was dissolved in 5 mL of toluene. $AlCl_3$ (0.12 g, 0.89 mmol), dissolved in 2 mL of

(17) Klingler, R. J.; Huffman, J. C.; Kochi, J. K. *J. Am. Chem. Soc.* **1980**, *102*, 208–216.
(18) Sanders, J. R. *J. Chem. Soc., Dalton Trans.* **1973**, *748*–749.
(19) Gargano, M.; Giannoccaro, P.; Rossi, M.; Vasapollo, G.; Sacco, A. *J. Chem. Soc., Dalton Trans.* **1975**, 9–12.
(20) Allison, J. D.; Walton, R. A. *J. Am. Chem. Soc.* **1984**, *106*, 163–168.
(21) Elson, I. H.; Kochi, J. K.; Klabunde, U.; Manzer, L. E.; Parshall, G. W.; Tebbe, F. N. *J. Am. Chem. Soc.* **1974**, *96*, 7374.
(22) Gaudiello, J. G.; Sharp, P. R.; Bard, A. J. *J. Am. Chem. Soc.* **1982**, *104*, 6373.

ether, was added with stirring. The blue precipitate was removed by filtration, washed with toluene and ether, and dried in vacuo; the yield was quantitative.

^1H NMR (CD_2Cl_2, 250 MHz, −50 °C): 1.75 (d, 18 H, J_{HP} = 7.9 Hz, PMe_3), 1.62 (s, 18 H, PMe_3'), −3.49 (structured quintet, ~2 H, $J \sim 40$ Hz, WH_2; see Figure S-1c). Simulation of the hydride region as an HH'AA'B_2 spin system (Figure S-1d) gave J_{HA} = 40 Hz, $J_{HA'}$ = 35 Hz, J_{HB} = 45 Hz, and J_{AB} = 0 Hz. ^{31}P NMR (CD_2Cl_2, 36.2 MHz, −40 °C): 4 (s with satellites, J_{PW} = 274 Hz, 2 PMe_3 or 2 PMe_3'), −6 (s with satellites, J_{PW} = 195 Hz, 2 PMe_3 or 2 PMe_3'). IR (Nujol; cm^{-1}): 1910 (m, WH).

Preparation of $[WCl(MeCN)H_2(PMe_3)_4]^+BF_4^-$ (3a). Solid $TlBF_4$ (0.26 g, 0.89 mmol) was added to a stirred solution of $WCl_2H_2(PMe_3)_4$ (0.5 g, 0.89 mmol) in 5 mL of MeCN. After 2 h, the mixture was filtered, the volume of the filtrate was reduced to 1 mL, and 3 mL of ether was added. Cooling to −40 °C for 3 h gave 0.30 g of yellow crystals. A second crop (0.15 g) was obtained from the mother liquor by a similar procedure; total yield 0.45 g (78%).

Anal. Calcd for $WC_{14}H_{41}BClF_4NP_4$: C, 25.73; H, 6.33. Found: C, 25.86; H, 6.42. ^1H NMR (CD_3CN, 270 MHz, 0 °C): 1.95 (s, 3 H, CH_3CN), 1.65 (d, 9 H, J_{HP} = 8.8 Hz, PMe_3), 1.54 (d, 9 Hz, J_{HP} = 8.4 Hz, PMe_3'), 1.49 (t, 18 H, J_{HP} = 3.6 Hz, 2 PMe_3''), −2.88 (m, ~2 H, WH_2). When the sample is warmed to 20 °C, the signals for PMe_3 and PMe_3' coalesce; $\Delta G^* = 15$ kcal mol^{-1}. $^{13}C\{^1H\}$ NMR (CD_3CN, 67.89 MHz, 0 °C): 88 (s, MeCN), 25 (d, J_{CP} = 33 Hz, PMe_3 and PMe_3'), 19 (t, J_{CP} = 15 Hz, PMe_3''), 2 (s, CH_3CN). The gated $^{13}C\{^1H\}$ spectrum gave J_{CH} = 128 Hz for the phosphines and J_{CH} = 136 Hz for CH_3CN. $^{31}P\{^1H\}$ NMR (CD_3CN, 36.2 MHz, −10 °C): −14 (dt with satellites, J_{PP} = 54 and 14 Hz, J_{PW} = 146 Hz, PMe_3), −23 (dt with satellites, J_{PP} = 54 and 14 Hz, J_{PW} = 181 Hz, PMe_3'), −26 (t with satellites, J_{PP} = 14 Hz, J_{PW} = 195 Hz, 2 PMe_3''). When the sample is warmed to 40 °C, the signals for PMe_3 and PMe_3' coalesce; $\Delta G^* = 15$ kcal mol^{-1}. Selectively decoupling the phosphine protons (109 MHz, −22 °C) turns the PMe_3 and the PMe_3' signals into overlapping tdt patterns (J_{PH} = 59 and 46 Hz) and the PMe_3'' signal becomes a complex pattern with $J_{PH} \sim 45$ Hz. IR (Nujol; cm^{-1}): 1960 (sh, WH), 1920 (m, br, WH).

Preparation of $[WCl_2H_2(PMe_3)_4]^+BF_4^-$ (1^+). (a) With Ferrocene of Crystallization. Ferrocenium tetrafluoroborate (0.27 g, 1 mmol) in 3 mL of MeCN was added dropwise with stirring to a solution of $WCl_2H_2(PMe_3)_4$ (0.56 g, 1 mmol) in 5 mL of MeCN. The resulting red solution was cooled to −40 °C overnight, and a small amount of ferrocene was removed by filtration. The filtrate was reduced to 2 mL, ether (3 mL) was added, and the mixture was cooled to −40 °C for 2 h. The resulting red-brown crystals (0.39 g) were removed by filtration. Another 0.15 g was obtained by similarly treating the filtrate; total yield 0.55 g (66%).

Anal. Calcd for $WC_{12}H_{38}BCl_2F_4P_4 \cdot FeC_{10}H_{10}$: C, 31.69; H, 5.80. Found: C, 31.95; H, 5.75. ^1H NMR (CD_3CN, 89.56 MHz): 4.17 (s, Cp_2Fe), 3.6 (s, $\Delta\nu_{1/2} \sim 400$ Hz, 2 PMe_3), −8.7 (s, $\Delta\nu_{1/2} \sim 1000$ Hz, 2PMe_3'). IR (Nujol; cm^{-1}): 1940 and 1920 (m, WH).

(b) Without Ferrocene of Crystallization. Ferrocenium tetrafluoroborate (0.27 g, 1 mmol) in 2 mL of MeCN was added dropwise with stirring to a solution of $WCl_2H_2(PMe_3)_4$ (0.56 g, 1 mmol) in 20 mL of toluene. The resulting red-orange microcrystalline precipitate was removed by filtration, washed with toluene and ether, and dried in vacuo; yield 0.52 g (80%). The product was shown to be ferrocene free by its ^1H NMR spectrum and CV.

Preparation of $[WCl(MeCN)H_2(PMe_3)_4]^{2+}(BF_4^-)_2$ ($3a^+$). $AgBF_4$ (80 mg, 0.41 mmol) in 3 mL of MeCN was added dropwise to a solution of $[WCl(MeCN)H_2(PMe_3)_4]^+BF_4^-$ (0.27 g, 0.41 mmol) in 5 mL of MeCN. The gray precipitate of Ag was removed by filtration. The filtrate was concentrated to ca. 2 mL and cooled to −40 °C for 1 h. Orange crystals (0.18 g) were collected by filtration. A second crop of 0.04 g was obtained by adding ether to the filtrate and cooling to −40 °C; total yield 0.22 g (73%). Only free CH_3CN was observed in its ^1H NMR spectrum in CD_3CN. IR (Nujol; cm^{-1}): 2300 and 2270 (m and s, MeCN), 1950 and 1930 (m and sh, WH). The product was identified by its CV.

Structure Analysis. An outline of crystallographic and data collection parameters is given in Table I. Crystals were grown by cooling a solution of the complex in MeCN to −40 °C. A crystal was selected and mounted in a glass capillary under dinitrogen. Cell dimensions were based upon a Delaunay reduction of a cell obtained from the centering of 25 reflections on the diffractometer.

Intensity data (294 K) were measured by the θ-2θ step-scan technique with Mo Kα radiation from a graphite monochromator. A total of 3035 Bragg reflections were measured. The intensities of three standard reflections were measured after each 7200-s exposure to the X-rays and were used to correct for the approximately 30% intensity decay that occurred during the experiment. The correction ranged from 0.98 to 1.23. Empirical absorption corrections were made with the ω-scan technique (μ = 44.2 cm^{-1}). Averaging of equivalent reflections gave 3035 data points of which 1733 had $F_o > \sigma(F_o^2/2F_o)$; these were used to refine the structure ($\sigma^2(F_o^2) = \sigma^2$(counting) + $(0.05F_o^2)^2$ and $\sigma(F_o) = \sigma(F_o^2)/2F_o$).

The structure was resolved by Patterson and Fourier methods. Least-squares refinement minimizing $\sum w(|F_o| - |F_c|)^2$, where $w = 1/\sigma^2(F_o)$, converged with $R = \sum||F_o| - |F_c||/\sum|F_o| = 0.055$ and $R_w = [\sum(|F_o| - |F_c|)^2/\sum wF_o^2]^{1/2} = 0.062$. Hydrogen atoms were placed in "ideal" X-ray positions. Those for the methyl groups were based on the location of at least one peak in a reasonable hydrogen atom position. Early in the refinement a disorder problem for the BF_4 ion became apparent. A single boron position and eight fluorine positions, or two orientations of the tetrahedron, were indicated. Attempted refinement of all these led to unreasonable bond lengths and angles. These positions were therefore fixed. Within the two tetrahedrons the bond distances ranged from 1.20 to 1.50 Å, and the bond angles ranged from 70 to 130°. The final difference Fourier map had the two largest peaks (0.78 and 0.77 e/Å^3) in the vicinity of the BF_4 ion. No extinction correction was applied. The maximum parameter shift on the last cycle was less than 0.03 times its esd, and the error in an observation of unit weight was 1.562. Atomic scattering factors were taken from ref 23. Final atomic positional parameters for the refined atoms are included in Table II. Selected interatomic bond distances and angles are given in Table III.

Acknowledgment. The authors thank Professor E. O. Schlemper for assistance with the structure determination, Professors D. Cowan and S. I. Weissman for the EPR spectra, and Professor R. R. Schrock for helpful discussions. Acknowledgment is made to the donors of the Petroleum Research Fund, administered by the American Chemical Society, for partial support of this research and to the National Science Foundation (Grant CHE-7820347) for partial purchase of the X-ray equipment.

Registry No. **1**, 87738-93-0; $\mathbf{1}^+ \cdot Cp_2Fe$, 95978-99-7; **2a**, 95978-93-1; **2b**, 95978-94-2; **3a**, 95978-96-4; $\mathbf{3a}^+$, 95979-01-4; $WCl_2(PMe_3)_4$, 76624-80-1; H_2, 1333-74-0.

Supplementary Material Available: A figure showing the hydride region of the ^1H NMR spectra of $WCl_2H_2(PMe_3)_4$ (**1**) and $[WClH_2(PMe_3)_4]^+$ (**2**) and their simulations, a packing diagram for $[WCl_2H_2(PMe_3)_4]^+BF_4^- \cdot Cp_2Fe$, a listing of structure factor amplitudes, a table of nonrefined atom positional parameters, a table of thermal parameters, and a least-squares plane table (16 pages). Ordering information is given on any current masthead page.

(23) "International Tables for Crystallography"; Kynoch Press: Birmingham, England, 1974; Vol. IV.